

NO-A179 924

VERIFICATION OF EOSAEL (ELECTRO-OPTICAL SYSTEMS

1/1

ATMOSPHERIC EFFECTS LIBRA (U) DEFENCE RESEARCH

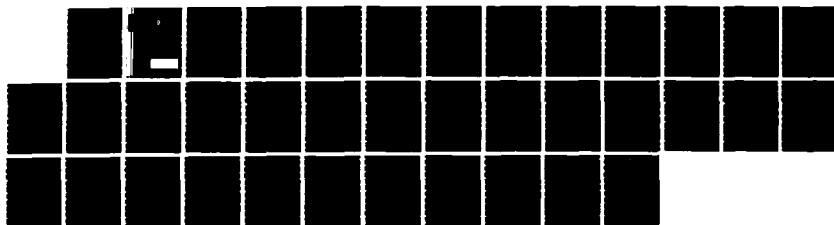
ESTABLISHMENT VALCARTIER (QUEBEC) D HUTT ET AL. MAR 87

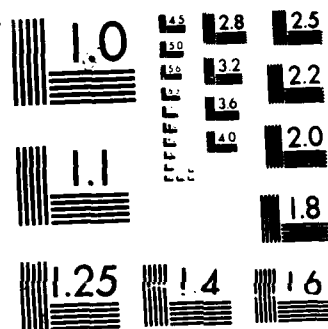
UNCLASSIFIED

DREV-R-4423/87

F/G 4/2

NL





MICROCOPY RESOLUTION TEST CHART
NATIONAL BUREAU OF STANDARDS 1963-A

DREV REPORT 4423/87
FILE: 3633A-011
MARCH 1987

CRDV RAPPORT 4423/87
DOSSIER: 3633A-011
MARS 1987

DTIC
ELECTE
APR 30 1987
S D

VERIFICATION OF EOSAEL SNOW TRANSMITTANCE PREDICTIONS

D. Hutt

R.C. Shirkey

DISTRIBUTION STATEMENT A

Approved for public release
Distribution Unlimited

RESEARCH AND DEVELOPMENT BRANCH
DEPARTMENT OF NATIONAL DEFENCE
CANADA

BUREAU - RECHERCHE ET DÉVELOPPEMENT
MINISTÈRE DE LA DÉFENSE NATIONALE
CANADA

Defence Research Establishment
Centre de recherches pour la Défense,
Valcartier, Québec

SANS CLASSIFICATION
DISTRIBUTION ILLIMITÉE

Canada

87 4 29 017

APR 22 1987

DREV R-4423/87
FILE: 3633A-011

UNCLASSIFIED

CRDV R-4423/87
DOSSIER: 3633A-011

VERIFICATION OF EOSAEL SNOW TRANSMITTANCE PREDICTIONS

by

D. Hutt and R.C. Shirkey*

* US Army Atmospheric Sciences Laboratory
Las Cruces, N.M., U.S.A.

DEFENCE RESEARCH ESTABLISHMENT
CENTRE DE RECHERCHES POUR LA DÉFENSE
VALCARTIER

Tel: (418) 844-4271

Québec, Canada

March/mars 1987

SANS CLASSIFICATION



Accession For	
NTIS CRA&I	<input checked="checked" type="checkbox"/>
DTIC TAB	<input type="checkbox"/>
Unannounced	<input type="checkbox"/>
Justification	
By	
Distribution /	
Availability Codes	
Dist	Avail and/or Special
A-1	

ABSTRACT

Measurements of atmospheric transmission during periods of snowfall were made in the visible and infrared during March and April 1985. The measurements are compared to transmission predicted by the XSCALE module of the Electro-Optical Systems Atmospheric Effects Library (EOSAEL). The XSCALE predictions correspond well with measured transmittances in the visible but predictions in the IR are considerably less than the measured values. This suggests that the snow transmittance algorithm used in XSCALE is more accurate for transmissometers whose receiver diameters are much larger than the beam diameter.

RÉSUMÉ

La mesure de la transmission atmosphérique dans le visible et l'infrarouge a été effectuée au cours de chutes de neige pendant la période mars-avril 1985. Les mesures sont comparées aux transmissions prédites par le module XSCALE du "Electro-Optical Systems Atmospheric Effects Library" (EOSAEL). Les prédictions de XSCALE correspondent bien aux transmittances mesurées dans le visible mais les prédictions dans l'IR sont considérablement moindres que les valeurs mesurées. Cela suggère que l'algorithme utilisé pour calculer la transmittance dans la neige est plus précis pour les transmissomètres dont le récepteur est beaucoup plus large que le diamètre du faisceau.

TABLE OF CONTENTS

ABSTRACT/RÉSUMÉ	1
LIST OF SYMBOLS	v
1.0 INTRODUCTION	1
2.0 INSTRUMENTATION	2
2.1 Transmission Range and Locale	2
2.2 Visible Transmissometer	2
2.3 Infrared Transmissometer	4
2.4 Meteorological Parameters	4
2.5 Aerosol Particle Concentration and Size Distribution ..	5
2.6 Snow Characterization	6
3.0 VISIBILITY AND VISIBLE TRANSMITTANCE	6
3.1 Observer Estimates of Visibility	6
3.2 Extinction Coefficient and Forward Scattering	7
4.0 XSCALE TRANSMITTANCE PREDICTIONS	10
4.1 The XSCALE Module	10
4.2 The Data	12
4.3 XSCALE Transmittance Estimates	15
4.4 Discussion of Results	19
5.0 THE XSCALE SNOW ALGORITHM	21
5.1 Effective Extinction Coefficient	21
5.2 Derivation of the Snow Algorithm	22
5.3 Detector Diameter vs Beam Diameter	25
6.0 CONCLUSIONS	27
7.0 ACKNOWLEDGEMENTS	28
8.0 REFERENCES	29

FIGURES 1 to 9

TABLES I to VIII

UNCLASSIFIED

v

LIST OF SYMBOLSNOTATIONDESCRIPTION

B	Fraction of total extinction due to snow
L	Length of transmission range
N	Number density of scattering particles
Q	Scattering efficiency of a particle
ΔQ	Perceived reduction in Q due to forward scattering
Q_{eff}	Effective extinction efficiency
\bar{Q}_{eff}	Effective extinction efficiency averaged over transmission range
RH	Relative humidity
T	Temperature
V	Visibility or meteorological range
l	Distance from receiver along transmission path
r	Radius of scattering particle
\bar{r}	Mean snow particle radius
r_d	Radius of transmissometer receiver
α	Volume extinction coefficient
$\hat{\alpha}$	Effective extinction coefficient along transmission path
α_f	Fog extinction coefficient
α_s	Snow extinction coefficient
α_{vis}	Extinction coefficient in the visible
η	Particle size parameter
θ_o	Angle subtended by receiver
λ	Wavelength of light
ρ	Phase function of scattering particles
τ	Total atmospheric transmittance
τ_{aer}	Transmittance due to atmospheric aerosols
τ_{vis}	Transmittance in visible band

1.0 INTRODUCTION

The Electro-Optical Systems Atmospheric Effects Library (EOSAEL) is a library of computer codes developed at the US Army Atmospheric Sciences Laboratory (ASL) which predict the effect of natural and battlefield gases, aerosols, smokes and dust on electro-optical system performance. EOSAEL, which is divided into 20 subprograms or modules, calculates extinction coefficients, atmospheric effects on radiation propagation and contrast reduction for wavelengths in the visible, infrared and millimeter wave regions. XSCALE is the EOSAEL module which calculates visible and IR transmittance under low visibility weather conditions such as fog, rain or snow.

In order to estimate transmittance through falling snow, the XSCALE algorithm requires as input the temperature, relative humidity, receiver radius and the visibility. An estimate of the mean snow particle radius is made based on the temperature, and the visibility is used to calculate the extinction coefficient along the transmission path. Since snow particles scatter strongly in the forward direction, the measured transmittance depends not only on the extinction coefficient but also on the size of the transmissometer receiver. The XSCALE algorithm is designed to take the effect of forward scattering into account based on the receiver radius.

In this report, estimates of transmittance in the visible and in the 3-5 μm and 8-12 μm bands are made using XSCALE and compared to actual transmittance measurements made at DREV under snowfall conditions.

This work was performed between March 1985 and January 1986 under the terms of a Memorandum of Understanding (MOU) between ASL and DREV. The work was performed under PCN 33A11, Aerosol Studies.

2.0 INSTRUMENTATION

2.1 Transmission Range and Locale

The transmission range is located at Defence Research Establishment Valcartier (DREV), situated approximately 20 km northwest of Quebec City. The local environment is rural. The receiver station is located on the top floor of a laboratory building with the receivers 9.4 m above the ground. The sources are sheltered in a hut at ground level, 538.4 m from the receivers along the 13° NW direction. The transmissometer path is slightly slanted at an angle of 1.43°. During the measurement period (between January and April 1985), the land below the transmission path was completely snow covered. The meteorological and aerosol sensors were located on the roof of the receiver station approximately 3 m above the receivers.

2.2 Visible Transmissometer

The visible transmissometer consists of a 10-mW HeNe laser source and a Fresnel lens/silicon detector receiver. The laser beam is chopped at a frequency of 480 Hz and collimated to a 5-cm-diameter beam. The demodulation reference signal is derived from the chopper and is transmitted to the receiver station by a small FM radio transmitter.

The receiver consists of a 25.4-cm-diameter $f/0.8$ Fresnel lens, a focal plane aperture and a $5 \times 5 \text{ cm}^2$ silicon detector positioned 1 cm behind the aperture (see Fig. 1). The focal plane aperture is used to limit the field of view of the receiver to 40 mrad. The detector output is connected to a low input impedance current-to-voltage converter which provides a voltage output proportional to the intensity of the incident radiation. Tests have shown that the receiver response to the modulated laser light is independent of the level of ambient light.

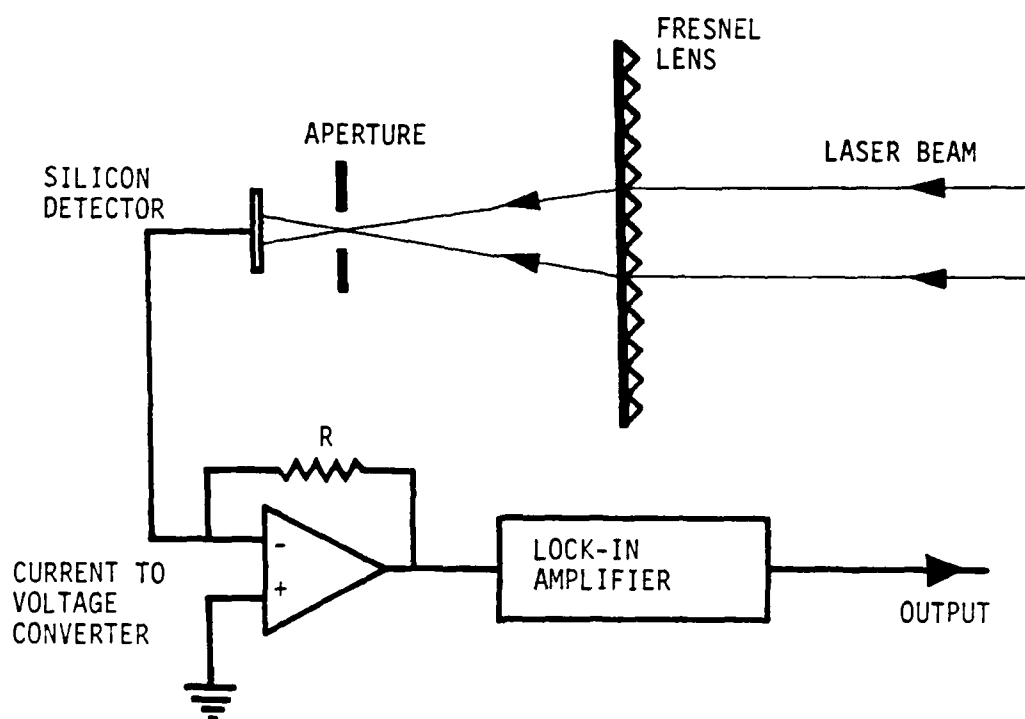


FIGURE 1 - Visible transmissometer receiver

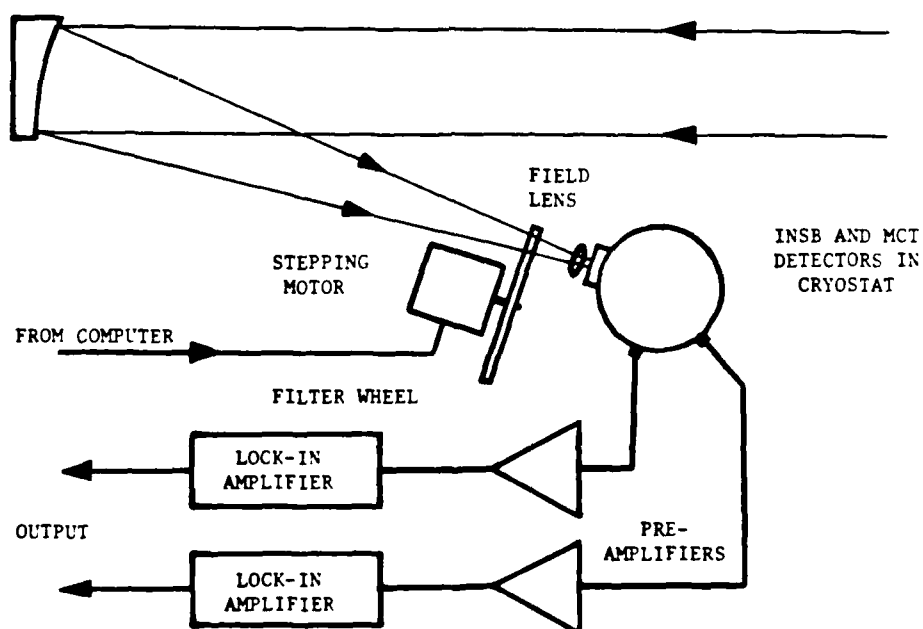


FIGURE 2 - IR transmissometer receiver

2.3 Infrared Transmissometer

The source of the DREV IR transmissometer is a Barnes model 14-708 IR source consisting of a 650°C blackbody, 90-Hz chopper wheel and 12.2-cm-diameter off-axis parabolic mirror which collimates the IR beam. The demodulation reference signal is derived from the chopper wheel and is transmitted to the receiver station by radio.

The receiver was developed at DREV and is shown in Fig. 2. The detector is an Infrared Industries InSb/HgCdTe sandwich detector. The radiation is collected by a 9.14-cm-diameter off-axis parabolic mirror and focused to a point in front of a 3-mm-diameter germanium field lens. The receiver field of view (FOV) is 6.0 mrad. The lens has an antireflection coating for the 8-14 μm band to enhance transmission to the less sensitive HgCdTe detector. The IR beam is intercepted near the focus by a filter wheel containing five filters of bandwidths: 3.4-4.1 μm , 4.5-5.0 μm , 3.0-5.0 μm , 8-12 μm and 10-12 μm . For this report, the measurements made with the relatively wide 3.0-5.0 μm and 8-12 μm filters will be used. The filters are advanced sequentially under the control of a microcomputer which also controls a data acquisition system. A transmission measurement is made using each filter approximately every 50 s. The calibration of both transmissometers is described in Ref. 1 and the absolute accuracy has been calculated to be 3% for the IR transmissometer and 1.5% for the visible transmissometer. The main specifications for the transmissometers are summarized in Table I.

2.4 Meteorological Parameters

Temperature, dew point, atmospheric pressure, wind speed and wind direction were measured using standard meteorological instruments. The sensors were mounted on the roof of the receiver station and the signals were continuously recorded along with the transmission data.

TABLE ISpecifications of IR and visible transmissometers

Quantity	Units	Transmissometers	
		Visible	Infrared
Collimator objective dia.	cm	$5 \pm .1$	$12.2 \pm .05$
Receiver objective dia.	cm	$25.4 \pm .1$	$9.14 \pm .05$
Collimator focal length	cm	$20 \pm .1$	$65 \pm .1$
Receiver focal length	cm	$20 \pm .5$	$63.4 \pm .1$
Source $\frac{1}{2}$ angle FOV	mrاد	$.05 \pm .01$	$5 \pm .1$
Receiver $\frac{1}{2}$ angle FOV	mrاد	20 ± 1	$3 \pm .1$
Range	m	538 ± 1	538 ± 1
Absolute accuracy	%	1.5	3

Some inconsistencies were experienced with the dew point meter which occasionally gave readings above the air temperature. However, during most measurement periods the dew point readings are considered accurate and agreed very well with measurements made at a nearby heliport.

2.5 Aerosol Particle Concentration and Size Distribution

The aerosol concentration and size distribution were measured with the Particle Measuring Systems model ASASP-300 active and model CSASP-100- HV classical probes. This arrangement provides particle concentration measurements in eight overlapping size ranges each divided into 15 resolution bins. The total range covers particles of $0.15 \mu\text{m}$ to $32 \mu\text{m}$ in diameter. The probes were installed on the roof of the receiver station. They were operated in the standard axial fan/accelerator horn configuration. To prevent snowflakes from being drawn

into the sample cavity, the accelerator horns were oriented downward. The probes were calibrated using a Devilbiss nebulizer which produces monodispersed spherical latex particles of known diameter.

2.6 Snow Characterization

Samples of falling snow crystals were preserved for visual inspection using the replica technique described in Ref. 1. The samples were usually taken at half-hour intervals. Using these samples, the types of snow crystals were identified and estimates made of the mean particle radius \bar{r} and standard deviation ϵ . The airborne snow mass concentration was also measured using the Airborne Snow Concentration Measuring Equipment (ASCME) built at DREV after the design of Lacombe (Ref. 2). This device provides a real-time measurement of the mass concentration of airborne snow which was recorded along with the transmission measurements. The ASCME is fully described in Refs. 2 and 3.

3.0 VISIBILITY AND VISIBLE TRANSMITTANCE

3.1 Observer Estimates of Visibility

Meteorological range or visibility is defined as the greatest distance at which it is possible to see and identify with the unaided eye: a) a prominent dark object against the horizon sky during the day and b) an unfocused, moderately intense light source during the night (Ref. 4). The vagueness of these definitions and the subjectiveness of individual observers means that visibility estimates are generally not very accurate. Unfortunately, in the field, visibility is often the only indication of the degree of atmospheric extinction. In the XSCALE module, visibility is an important parameter in the prediction of IR transmittance.

An empirical formula that relates visibility V to the visible extinction coefficient a_{vis} is Koschmeider's formula:

$$V = \frac{3.912}{a_{vis}} \quad . \quad [1]$$

Equation 1 may be combined with Beer's law,

$$\tau = e^{-La} \quad [2]$$

to obtain a relation between visibility and visible transmittance τ_{vis} , i.e.

$$V = - \frac{3.912 L}{\ln \tau_{vis}} \quad [3]$$

where L is the length of the transmission path. Figure 3 is a scatter plot of observer estimates of visibility vs visibility derived from visible transmittance measurements using eq. 3. The error in the observer-estimated visibility is about 35%.

To eliminate the subjective element of observer visibility estimates, the XSCALE snow algorithm is tested in Chapter 4.0 using values of visibility derived from the measured visible transmittance using eq. 3.

3.2 Extinction Coefficient and Forward Scattering

Beer's law is exact only for an ideal receiver with an infinitely small field of view. For real receivers with a finite field of view operating in a medium with extinction coefficient a , off-axis contributions to the detected light can result in a measured transmittance that is considerably greater than that given by eq. 2.

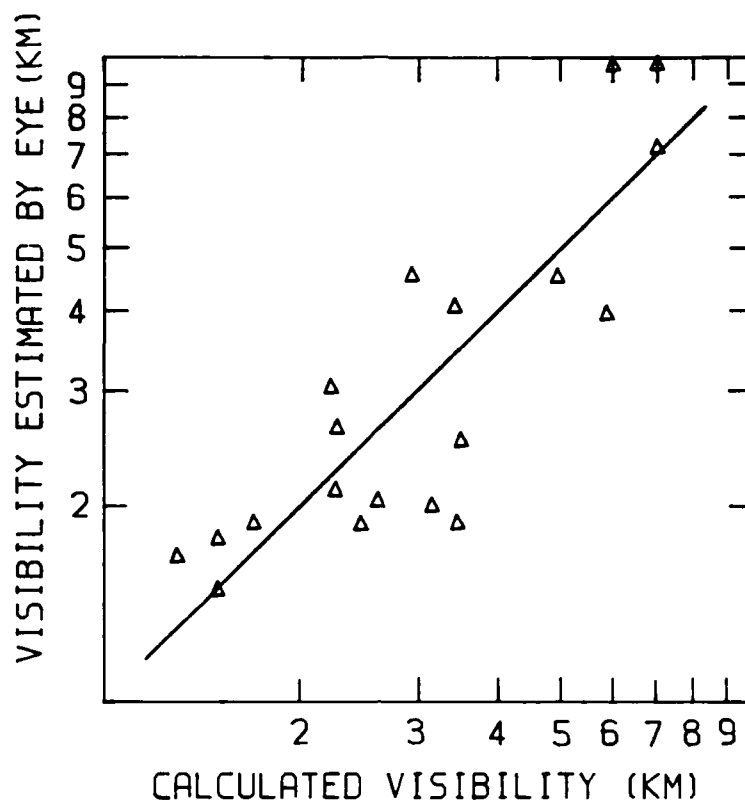


FIGURE 3 - Visibility estimated by an observer vs visibility derived from visible transmittance measurements using eq. 3

Snow particles are generally larger than IR and visible wavelengths and thus a large fraction of the energy scattered by snow is contained in a narrow forward lobe (Ref. 5). Since the angular width of the forward scattering lobe is of the same order as typical transmissometer receivers, forward scattering can contribute greatly to snow transmittance measurements depending on particle size, wavelength and transmissometer design.

TABLE IIForward scattering correction to measured transmittance

Measured Transmittance	Corrected Transmittance		
	4 μm	10 μm	0.633 μm
1.0	1.0	1.0	1.0
0.9	.86	.88	.89
0.7	.61	.65	.68
0.4	.29	.33	.37
0.2	.12	.14	.18
0.1	.05	.06	.07

The component of measured transmittance due to forward scattering was computed using the Mill and Shettle model (Ref. 6). The "corrected" transmittance or the transmittance of the unscattered beam was found by subtracting the forward scattering component from the measured transmittance. Examples of measured transmittances and the corresponding forward scattering corrected values are given in Table II. The calculations were done with an assumed snow particle radius of 0.5 mm. See Ref. 1 for details.

Table II shows that the fraction of transmittance due to forward scattering increases as the transmittance decreases. The average percent difference between measured and corrected values is 27% at 4 μm and 18% at 10 μm . Therefore, the contribution of forward scattering to the measured transmittance is 1.5 times greater at 4 μm than at 10 μm . The effect of forward scattering on the visible transmissometer is much less than that on the IR transmissometer with an average percent

difference between measured and corrected visible transmittance of 10%. This has been attributed to the fact that the visible transmissometer beam is much smaller in diameter than the receiver.

Extinction coefficients calculated with eq. 2 using corrected transmittance measurements should be closer to the true values than those derived from uncorrected measurements. In Chapter 4.0, values of visibility used by XSCALE are derived from corrected visible transmittance measurements.

4.0 XSCALE TRANSMITTANCE PREDICTIONS

4.1 The XSCALE Module

The EOSAEL module XSCALE is a self-contained FORTRAN program that can estimate visible and IR transmission during low visibility weather conditions. XSCALE calculates transmittance through fog, rain and snow using various empirical and semiempirical models. The transmittance component due to background aerosols is calculated using Mie

TABLE III

Data required for XSCALE transmittance calculation

Input	(units)	Output	(units)
Wavelength	(μm)	Extinction coefficient	(km^{-1})
Transmission path length	(km)	Transmission	(%)
Visibility	(km)		
Receiver radius	(cm)		
Temperature	(°C)		
Relative humidity	(%)		

theory and model aerosol size distributions based on size distributions measured in many common air mass types (Ref. 7). The data required by XSCALE to make horizontal path transmittance measurements are listed in Table III along with the computation results.

The extinction coefficient α_s due to the snow particles is calculated using the formula

$$\alpha_s = \left(\frac{1.96}{V} \right) (1 + e^{-0.88k}) \quad [4]$$

where $k = 2\pi \bar{r} r_d / \lambda V$ (Ref. 5). In eq. 4, V is the visibility, r_d is the receiver radius, λ is the wavelength and \bar{r} is the mean snow particle radius. \bar{r} is estimated using the empirical relations given in Table IV.

TABLE IV

XSCALE snow particle radius vs temperature

Radius \bar{r} (μm)	Temperature T ($^{\circ}\text{C}$)
100	$T < -15$
$250 + 10T$	$-15 < T < 0$
$250 + 25T$	$0 < T < 2$
300	$T > 2^{\circ}$

XSCALE uses one of two possible background aerosol models for snow transmittance estimates. The model used is chosen automatically by XSCALE based on the input relative humidity. For humidity less than 95%, the aerosol model is one associated with dry snow and contributes little to visible or IR extinction. For humidity greater than 95%, a background of advective fog is assumed. The fraction of total extinction due to the fog depends on the concentration of the fog particles. The total extinction α may be expressed as the sum of relative extinction contributions due to fog and snow, i.e.

$$\alpha = (1 - B) \alpha_f + B \alpha_s$$

where α_f is the fog extinction coefficient and the factor B is calculated using the empirical relation

$$B = -0.025 T + 0.23 V^{-1} - 0.021 RH + 2.47. \quad [5]$$

In eq. 5, T is the temperature, V is the visibility and RH is the relative humidity.

After the extinction contributions due to snow particles and the aerosol background are determined, the transmission along the path length L is calculated using Beer's law and the calculated total extinction coefficient.

4.2 The Data

The visible and IR transmittance data used to verify the XSCALE snow algorithm were collected on March 1 and April 2 and 3, 1985. Time plots of these data are shown in Figs. 4 through 6. The extinction due to molecular absorption has been removed from the transmittance data by normalizing them to molecular transmittances calculated using LOWTRAN

as described in Ref. 1. Thus the transmittance curves in Figs. 4-6 are due to extinction by airborne snow and the aerosol background. Figures 4-6 also show the airborne snow mass concentration measured with the ASCME device described in Refs. 2 and 3. The snow concentration curves indicate the intensity of the snow episode where a snow concentration of 500 mg per cubic meter of air is considered a very heavy snowfall.

The transmittance component due to the background aerosols was calculated using the measured aerosol size distribution and Mie theory as described in Ref. 1. The results show that for the snow episodes of April 2 and 3, attenuation in the visible due to aerosols is slight, with the visible aerosol transmittance being greater than 0.97. IR extinction due to aerosols is negligible on these days. The aerosol measurements indicate that on March 1 there was a higher aerosol concentration but the transmittance due to background aerosols was greater than 0.93 in all bands. The aerosol size distributions measured between 10:00 and 11:00 on April 2 and 18:00 to 19:00 on April 3 are shown in Figs. 7a and 7b.

The temperature, relative humidity and visibility data used as input to XSCALE are found in Table V along with aerosol visible transmittance τ_{aer} derived from the aerosol concentration measurements. On March 1 and April 3, the measured relative humidity was between 99 and 100% although the values indicated in Table V are 95%. The reason for this substitution was to avoid invoking the XSCALE advective fog background aerosol model. The aerosol visible transmittance values in Table V show that the extinction due to aerosols was small for all three days. Therefore, the advective fog model which produces high extinctions would be inappropriate. Thus all transmittance predictions made with XSCALE use the dry snow aerosol model.

As discussed in Section 3.2, the visibility values are derived from the forward scatter corrected visible transmittance measurements using eq. 3.

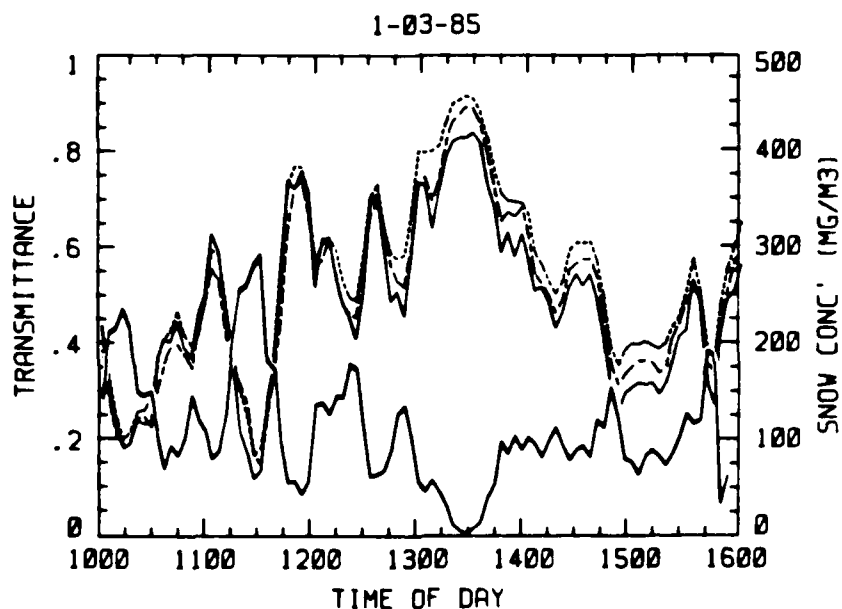


FIGURE 4 - Visible transmittance, IR transmittance and snow mass concentration for March 1, 1985

— Visible - - - - - 3-5 μ m
- . - . - 8-12 μ m — snow mass concentration

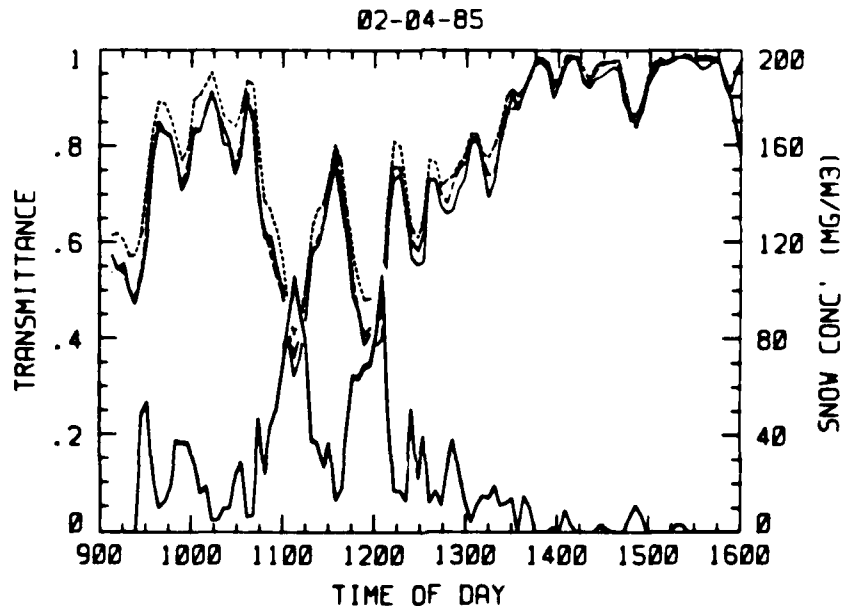


FIGURE 5 - Visible transmittance, IR transmittance and snow mass concentration for April 2, 1985

— Visible - - - - - 3-5 μ m
- . - . - 8-12 μ m — snow mass concentration

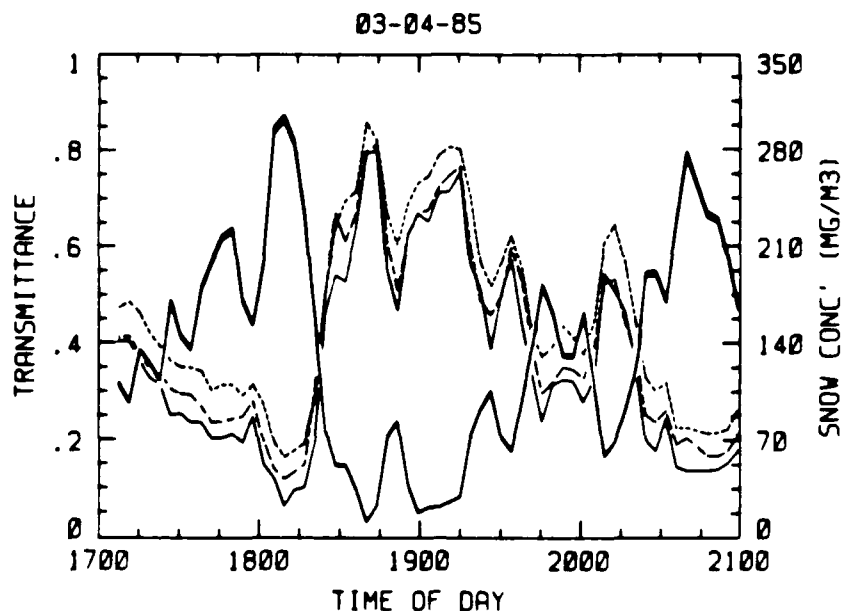


FIGURE 6 - Visible transmittance, IR transmittance and snow mass concentration for April 3, 1985

—— Visible - - - - - 3-5 μ m - . - . - 8-12 μ m ——— snow mass concentration

4.3 XSCALE Transmittance Estimates

Using the data of Table V and a path length of 0.538 km, estimates of transmittance at 0.63 μ m, 4 μ m and 10 μ m were made using XSCALE. For the IR predictions, the receiver radius was 4.57 cm and for the visible predictions, the receiver radius was 12.7 cm. In Table VI, the results are compared to the transmittances measured at 0.63 μ m and in the 3-5 μ m and 8-12 μ m bands.

At 0.63 μ m the XSCALE transmittance estimates agree very well with the measured values for all three snow episodes. However, at 4 μ m the calculated transmittances are on average 15% lower than the measured values for March 1 and April 2. On April 3, the visibility was

UNCLASSIFIED

16

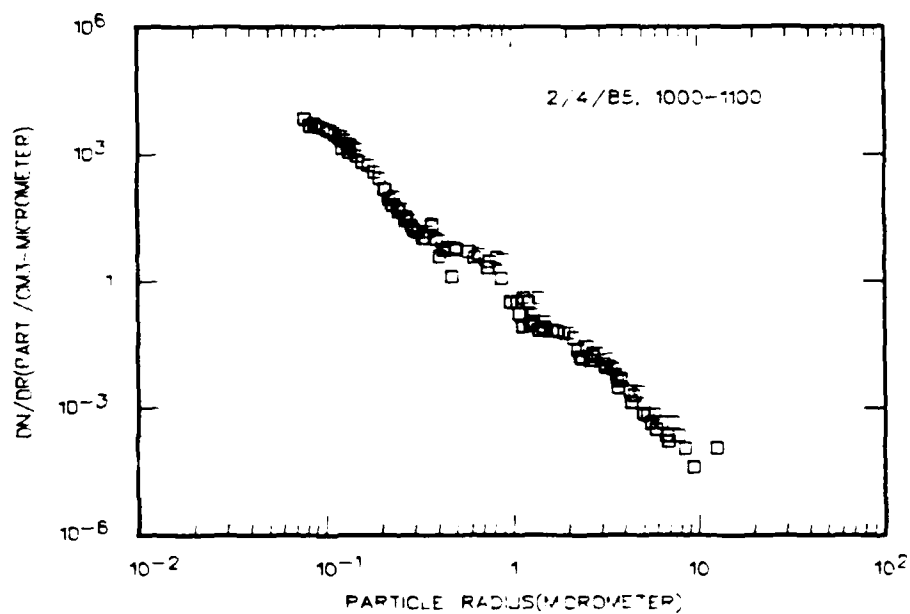


FIGURE 7a - Aerosol size distribution measured between 10:00 and 11:00 on April 2, 1985

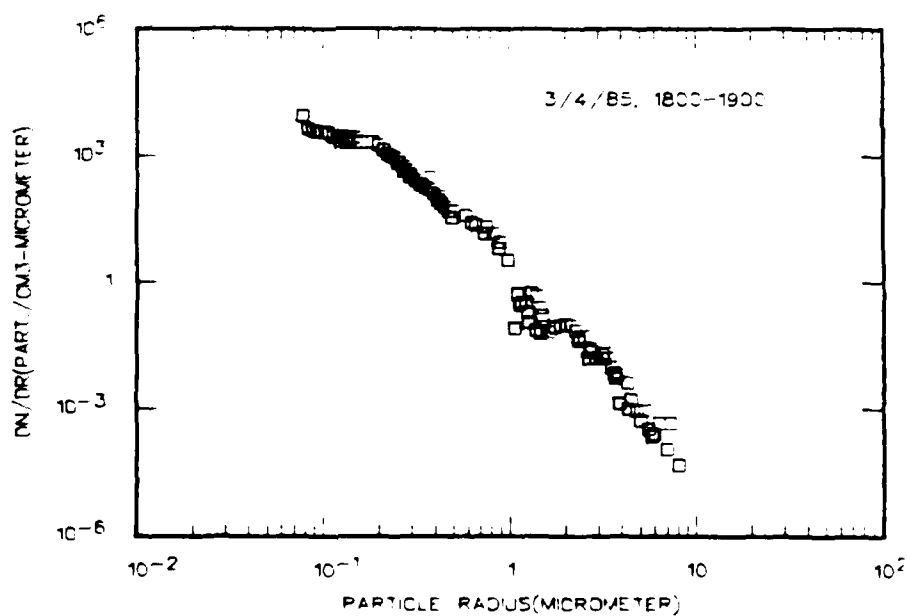


FIGURE 7b - Aerosol size distribution measured between 18:00 and 19:00 on April 3, 1985

TABLE VMeteorological data during snow episodes

Time	Visibility	Temperature (°C)	Relative Humidity (%)	τ_{aer} ($\lambda = .63 \mu m$)
March 1, 1985				
10:30	1.3	-2.2	95	.97
11:00	2.7	-2.1	95	.96
11:30	.94	-2.1	95	.95
12:00	3.1	-2.0	95	.94
12:30	2.7	-2.0	95	.94
13:00	5.9	-2.1	95	.94
14:30	3.2	-1.8	95	.94
15:00	1.6	-1.6	95	.94
15:30	2.2	-1.6	95	.93
April 2, 1985				
10:00	6.4	-3.3	86	-
10:30	6.4	-3.3	88	-
11:00	3.1	-2.7	86	.99
11:30	5.5	-2.9	87	.99
12:00	2.1	-2.8	86	.99
12:30	3.3	-2.8	85	.99
13:00	6.2	-2.5	85	.99
April 3, 1985				
17:30	1.5	-2.0	95	.97
18:00	1.0	-2.4	95	.96
19:45	1.4	-2.6	95	.97
20:00	1.5	-2.8	95	.97
20:30	1.1	-2.6	95	-
20:45	1.0	-2.6	95	-
21:00	1.1	-2.6	95	-

TABLE VIMeasured and calculated snow transmittance

Time	0.63 μm Meas.	0.63 μm Cal.	3-5 μm Meas.	4 μm Cal.	8-12 μm Meas.	10 μm Cal.
March 1, 1985						
10:30	.23	.24	.28	.20	.23	.20
11:00	.49	.48	.48	.46	.49	.46
11:30	.13	.14	.18	.11	.15	.11
12:00	.51	.50	.56	.48	.57	.48
12:30	.49	.48	.56	.46	.55	.46
13:00	.72	.71	.78	.70	.75	.70
14:30	.54	.53	.59	.51	.57	.51
15:00	.30	.31	.39	.27	.36	.27
15:30	.42	.41	.49	.39	.49	.39
April 2, 1985						
10:00	.74	.73	.80	.72	.77	.72
10:30	.74	.73	.84	.72	.75	.72
11:00	.51	.50	.57	.48	.50	.48
11:30	.70	.69	.73	.68	.73	.68
12:00	.39	.39	.48	.36	.41	.36
12:30	.56	.55	.61	.53	.58	.53
13:00	.73	.72	.78	.71	.77	.71
April 3, 1985						
17:30	.26	.27	.35	.23	.30	.23
18:00	.15	.16	.28	.13	.20	.13
19:45	.24	.25	.37	.21	.30	.21
20:00	.28	.29	.38	.25	.33	.25
20:30	.18	.19	.30	.16	.24	.16
20:45	.14	.15	.21	.12	.17	.12
21:00	.18	.19	.26	.16	.21	.16

considerably less than on the other two days and the estimated 4- μ m transmittance is on average 41% less than the measured values. The results are similar in the 8-12 μ m band with the average calculated transmittances less than the measured values by about 20%.

4.4 Discussion of Results

Atmospheric transmittance measurements made through falling snow may include a large component due to forward scattered light. This forward scattering component was removed from the visible transmittance data using the method described in Section 3.3 of Ref. 1. The visibility data given in Table V are derived from the corrected visible transmittance using eq. 3. Since the XSCALE estimates of visible transmittance are very close to the measured values, it appears that the XSCALE snow algorithm has determined the contribution of forward scattering in the visible transmittance measurements.

TABLE VII

Forward scatter corrected (FSC) transmittance and XSCALE predictions

Time	4 μ m			10 μ m		
	Measured	FSC	XSCALE	Measured	FSC	XSCALE
April 3, 1985						
17:30	.35	.24	.23	.30	.24	.23
18:00	.28	.18	.13	.20	.15	.13
19:45	.37	.26	.21	.30	.24	.21
20:00	.38	.27	.25	.33	.26	.25
20:30	.30	.24	.16	.24	.18	.16
20:45	.21	.13	.12	.17	.12	.12
21:00	.26	.17	.16	.21	.16	.16

At 4 μm and 10 μm , the XSCALE estimates of transmittance are much lower than the measured values. Table VII compares some of the XSCALE estimates at 4 μm and 10 μm with the measured transmittance, and the measured transmittance with the forward scattered component removed.

At 4 μm , the XSCALE predictions are on average about 15% less than the forward scatter corrected values and about 40% less than the measured values. At 10 μm , the XSCALE values are about the same as the forward scatter corrected values and 23% lower than the measurements. Since the XSCALE transmittance predictions are consistently less than the measured values but close to the forward scatter corrected values, it appears that the XSCALE snow algorithm underestimates the contribution of forward scattering in the IR transmittance measurements.

According to Table IV, which gives \bar{r} as a function of temperature, the mean snow particle radius used by XSCALE in the calculations was about 230 μm for all three snow episodes. Values of snow particle radius determined by analyzing replicas of the snow crystals taken during each snowfall are given in Table VIII with the standard deviation.

TABLE VIII

Observed snow particle radius \bar{r}

Episode	\bar{r} (μm)	Std. dev.
March 1, 1985	1600	1100
April 2, 1985	900	700
April 3, 1985	800	500

A meaningful representative radius for snow particles is difficult to ascertain since the range of particle sizes is very large and the particles are irregularly shaped. However, Table VIII shows that the mean radius of snow particles observed during the three episodes are much larger than the 230 μm used in the XSCALE calculation. Furthermore, when using the Mill and Shettle forward scattering calculation, as described in Ref. 1, optimal results were achieved using $\bar{r} = 500 \mu\text{m}$. Use of an uncharacteristically small value for \bar{r} by XSCALE could explain why the algorithm underestimates the forward scattering contribution to the measured transmittance.

5.0 THE XSCALE SNOW ALGORITHM

5.1 Effective Extinction Coefficient

An ideal transmissometer has a receiver with an infinitely small field of view. Transmittance measurements made with such a transmissometer are related to the volume extinction coefficient of the medium exactly according to Beer's law,

$$\tau = e^{-L\alpha} \quad [6]$$

where α is the extinction coefficient and L the transmission path length. For a receiver with a finite field of view, the measured transmittance may be larger due to off-axis light scattered into the receiver. The extinction coefficient calculated using such measurements and eq. 6 is thus the apparent or effective extinction coefficient $\hat{\alpha}$, which is smaller than α depending on the fraction of forward scattered energy collected by the receiver.

In order to estimate transmittance through falling snow, the XSCALE model calculates the effective extinction coefficient $\hat{\alpha}$ and

derives the transmittance from eq. 6. A derivation of the XSCALE snow algorithm developed by Seagraves (Ref. 5) is summarized in the following section.

5.2 Derivation of the Snow Algorithm

The detection of forward scattered light by a receiver contributes to the measured transmittance and makes the particles appear to be less effective scatterers or to have a smaller extinction efficiency. Seagraves defines an effective extinction efficiency

$$Q_{\text{eff}} = Q - \Delta Q \quad [7]$$

where ΔQ is the reduction in Q_{eff} due to forward scattering. As shown in Fig. 8, a receiver of radius r_d subtends an angle θ_o at a point l on the beam axis.

For a particle at l , ΔQ is found by integrating the phase function $\rho(\theta)$ of the particle over the solid angle subtended by the receiver, i.e.

$$\Delta Q(\theta_o) = 2\pi \int_0^{\theta_o} \rho(\theta) \sin\theta d\theta. \quad [8]$$

The phase function used to evaluate eq. 8 is

$$\rho(\theta, \eta) = \frac{\eta^2}{4\pi} \left(\frac{2J_1(\eta \sin\theta)}{\eta \sin\theta} \right)^2 \quad [9]$$

where η is the particle size parameter equal to $2\pi r/\lambda$ and J_1 is the first-order Bessel function of the first kind. $\rho(\theta, \eta)$ is an approximate phase function derived from Mie theory and applies to homogeneous spheres larger than the wavelength (Ref. 8).

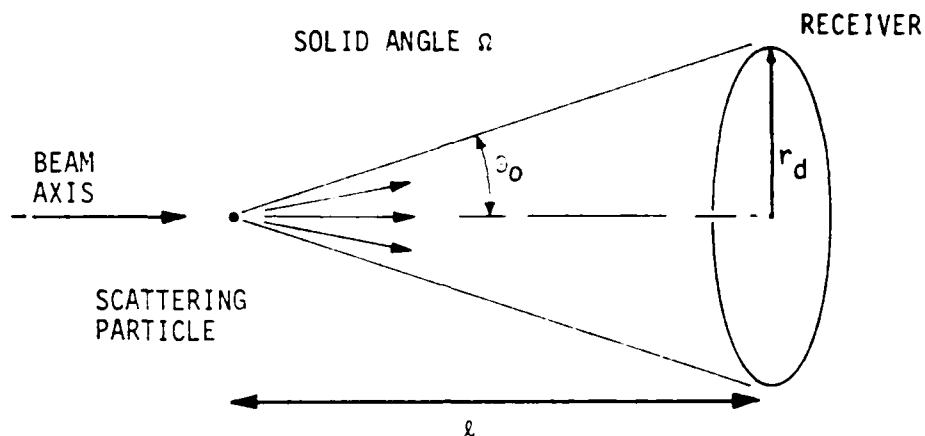


FIGURE 8 - Geometry used to calculate forward scattering contribution in XSCALE snow algorithm

Hodkinson found that the forward diffraction lobe for randomly oriented nonspherical particles was similar to that of spheres of equal geometric cross section (Ref. 9), so that $\rho(\theta, n)$ may be considered a reasonable approximation to the phase function of snow particles. Evaluating the integral in eq. 8 yields

$$\Delta Q(\theta_0) = 1 - J_0^2(n \sin \theta_0) - J_1^2(n \sin \theta_0). \quad [10]$$

Since $\sin \theta_0 = r_d / L \Delta Q(\theta_0)$ is a function of distance along the transmission path and receiver radius, forward scattering contributions from particles distributed along the beam axis may be accounted for by calculating a mean extinction efficiency \bar{Q}_{eff} . This is found by integrating ΔQ with respect to L along the beam path and subtracting it from $Q(\lambda, r)$, i.e.

$$\bar{Q}_{eff} = Q(\lambda, r) - \frac{1}{L} \int_0^L \Delta Q(L) dL, \quad [11]$$

where L is the length of the transmission path. Since snow particles are generally larger than visible and IR wavelengths, $Q(\lambda, r)$ is taken to be equal to 2. Seagraves gives an approximate solution to eq. 11 as

$$\overline{Q}_{\text{eff}} \cong e^{(-0.88 \frac{\pi r_d}{L})} + 1. \quad [12]$$

Note that as r_d becomes vanishingly small, $\overline{Q}_{\text{eff}}$ becomes equal to 2 which means that this model predicts that forward scattering effects are negligible for a sufficiently small receiver. The effective extinction coefficient $\hat{\alpha}$ is then found by substituting $\overline{Q}_{\text{eff}}$ in the definition of the extinction coefficient.

$$\alpha = Q \int_0^{\infty} \frac{dN}{dr} \pi r^2 dr, \quad [13]$$

where N is the number density function of the particles. Combining eqs. 12 and 13 yields

$$\hat{\alpha} = [e^{(-0.88 k)} + 1] \int_0^{\infty} \frac{dN}{dr} \pi r^2 dr \quad [14]$$

where $k = \pi r_d / L$. Using eq. 14, the ratio of $\hat{\alpha}$ for any two wavelengths may be written

$$\frac{\hat{\alpha}_1}{\hat{\alpha}_2} = \frac{1 + e^{(-0.88 k_1)}}{1 + e^{(-0.88 k_2)}}. \quad [15]$$

In order to relate $\alpha(\lambda)$ to visibility, the $\overline{Q}_{\text{eff}}$ of the human eye is taken to be equal to 2 since it is a very small receiver. The visible extinction coefficient is given by Koschmeider's formula as

$$\alpha_{vis} = \frac{3.912}{V} . \quad [16]$$

Combining eqs. 15 and 16 yields the effective extinction coefficient

$$\tilde{\alpha}(k,V) = \frac{1.96}{V} (1 + e^{-0.88k}). \quad [17]$$

Substituting $\tilde{\alpha}$ in Beer's law we obtain the XSCALE snow transmittance algorithm

$$\tau(k,L,V) = \exp \left\{ - \frac{1.96L}{V} (1 + e^{-0.88k}) \right\}. \quad [18]$$

In the XSCALE code (EOSAEL version 1984), the coefficient k has the value $\pi r_d^2/V$.

5.3 Detector Diameter vs Beam Diameter

The effective extinction efficiency \bar{Q}_{eff} defined in eq. 11 accounts for reduced extinction due to light forward scattered within a solid angle $\pi r_d^2/l^2$ about the forward direction as shown in Fig. 8. This means that only contributions from scatterers near the beam axis are accounted for. For a transmissometer whose beam width is smaller than the diameter of the receiver this should be a realistic model. In Chapter 4.0, XSCALE visible transmittance estimates are shown to agree very well with measured values. The visible transmittance was measured using a narrow beam transmissometer with the beam diameter one tenth the receiver diameter. The good agreement between predicted and measured transmittance in the visible indicates that the model is a good representation of a narrow beam transmissometer.

As discussed in Section 3.2, the visibility data used for the XSCALE calculations were derived from the measured visible transmittance from which the forward scattered contribution was removed using the method of Mill and Shettle (Ref. 6). The fact that the XSCALE

visible transmittance predictions are very close to the measured visible transmittance means that the XSCALE estimate of the forward scattering contribution in the visible agrees very closely with the Mill and Shettle model.

For transmissometers with a beam much larger than the receiver, forward-scattered energy may be received from particles far from the beam axis as illustrated in Fig. 9. It seems likely that for wide-beam transmissometers the effective extinction efficiency calculated in eq. 11 will be too large since only the forward scattering contributions of particles near the beam axis are acknowledged. This is supported by the fact that the XSCALE predictions in the IR were consistently below the measured values in both the 3-5 μm and 8-12 μm bands, suggesting that XSCALE underestimated the magnitude of the forward-scattered transmittance component.

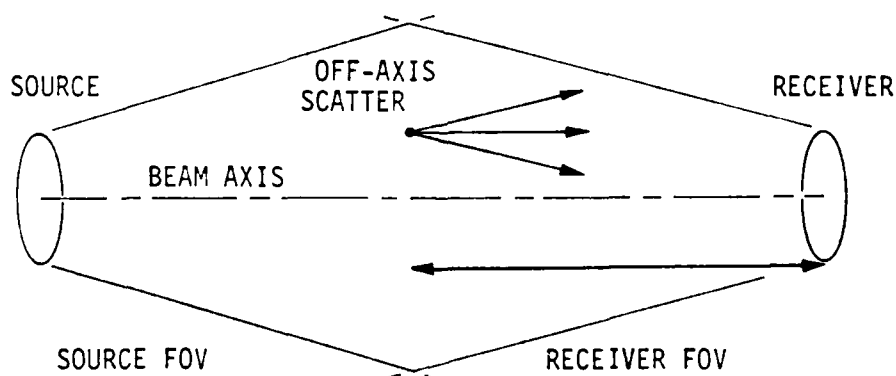


FIGURE 9 - Transmissometer with beam much larger than the receiver

6.0 CONCLUSIONS

Estimates of transmittance through falling snow made by the EOSAEL module XSCALE were compared to measurements of visible and IR transmittance made at DREV. The XSCALE algorithm requires as input the visibility which was derived from measurements of visible transmittance using the Beer and Koschmieder laws. The visible transmittance values used to calculate the visibility were corrected for forward scattering effects using the Mill and Shettle algorithm (Ref. 6). Using the derived visibility values as input, the XSCALE predictions of visible snow transmittance agreed very well with measurements made using a narrow-beam laser transmissometer with a receiver larger than the beam.

XSCALE predictions of snow transmittance in the IR were on average about 30% less than the measured values in the 3-5 μm band and about 20% less than measured values in the 8-12 μm band. This could be due in part to the fact that the XSCALE algorithm uses a mean particle radius which is much smaller than those observed during the snow transmittance measurements. The IR transmittance measurements were made using a transmissometer with a divergent beam much wider than the receiver at the receiver end.

It has also been shown that in calculating the forward-scattered transmittance component, the XSCALE algorithm does not take into account the contribution of scatterers found far from the beam axis. This could explain why XSCALE underestimates the forward-scattered component for transmissometers with a beam much wider than the receiver since scatterers far from the beam axis can contribute greatly to the energy collected by the receiver. On the other hand, the fact that the XSCALE predictions are very close to the measured visible transmittances shows that the algorithm is a good representation of a narrow-beam transmissometer whose beam is much smaller than the receiver diameter.

UNCLASSIFIED

28

7.0 ACKNOWLEDGEMENTS

The authors gratefully acknowledge the many helpful suggestions made by L. Bissonnette, who reviewed a draft of this report.

8.0 REFERENCES

1. Hutt, D.L., Bissonnette, L. and St-Germain, D., "Extinction of Infrared and Visible Radiation Due to Airborne Snow", DREV R-4414/86, May 1986, UNCLASSIFIED
2. Lacombe, J., "Airborne Snow Concentration Measuring Equipment", SNOW Symposium I, CRREL Special Report, p. 27, 1981.
3. Hutt, D.L., Bissonnette, L. and Oman, J., "The Measurement of Airborne Snow Mass Concentration", DREV R-4454, UNCLASSIFIED
4. McCartney, J., "Optics of the Atmosphere", Wiley, Toronto, 1976.
5. Seagraves, M.A., "Visible and Infrared Extinction Due to Falling Snow: An Approximate Model", ASL-TR-0158, US Army Atmospheric Sciences Laboratory, White Sands Missile Range, N.M., 1984.
6. Mill, J.D. and Shettle, E.P., "A Preliminary LOWTRAN Snow Model", SNOW Symposium II, CRREL Special Report, p. 239, 1983.
7. Richardson, M.B. et al, "Natural Aerosol Extinction Module XSCALE", ASL-TR-0160-7, US Army Atmospheric Sciences Laboratory, White Sands Missile Range, N.M., 1984.
8. Hodkinson, J.R. and Greenleaves, L., "Computations of Light Scattering and Extinction by Spheres According to Diffraction and Geometrical Optics, and Some Comparisons with the Mie Theory", J. Opt. Soc. Am., 53:577-588, 1963.
9. Hodkinson, J.R., "Light Scattering and Extinction by Irregular Particles Larger than the Wavelength", Electromagnetic Scattering, M. Kerker, editor, Macmillan, New York, pp. 87-100, 1963.

<p>CRDV R-4423/87 (SANS CLASSIFICATION)</p> <p>Bureau - Recherche et Développement, MDN, Canada. CRDV, C.P. 8800, Courcellette, Qué. G0A 1R0</p> <p>"Vérification des calculs EOSAEL de transmittance dans la neige" par D. Hutt et R.C. Shirkey</p> <p>La mesure de la transmission atmosphérique dans le visible et l'infrarouge a été effectuée au cours de chutes de neige pendant la période mars-avril 1985. Les mesures sont comparées aux transmissions prédites par le module XSALF du "Electro-Optical Systems Atmospheric Effects Library" (EOSAEL). Les prédictions de XSALF correspondent bien aux transmittances mesurées dans le visible mais les prédictions dans l'IR sont considérablement moindres que les valeurs mesurées. Cela suggère que l'algorithme utilisé pour calculer la transmittance dans la neige est plus précis pour les transmissomètres dont le récepteur est beaucoup plus large que le diamètre du faisceau.</p>	<p>CRDV R-4423/87 (SANS CLASSIFICATION)</p> <p>Bureau - Recherche et Développement, MDN, Canada. CRDV, C.P. 8800, Courcellette, Qué. G0A 1R0</p> <p>"Vérification des calculs EOSAEL de transmittance dans la neige" par D. Hutt et R.C. Shirkey</p> <p>La mesure de la transmission atmosphérique dans le visible et l'infrarouge a été effectuée au cours de chutes de neige pendant la période mars-avril 1985. Les mesures sont comparées aux transmissions prédites par le module XSALF du "Electro-Optical Systems Atmospheric Effects Library" (EOSAEL). Les prédictions de XSALF correspondent bien aux transmittances mesurées dans le visible mais les prédictions dans l'IR sont considérablement moindres que les valeurs mesurées. Cela suggère que l'algorithme utilisé pour calculer la transmittance dans la neige est plus précis pour les transmissomètres dont le récepteur est beaucoup plus large que le diamètre du faisceau.</p>
<p>CRDV R-4423/87 (SANS CLASSIFICATION)</p> <p>Bureau - Recherche et Développement, MDN, Canada. CRDV, C.P. 8800, Courcellette, Qué. G0A 1R0</p> <p>"Vérification des calculs EOSAEL de transmittance dans la neige" par D. Hutt et R.C. Shirkey</p> <p>La mesure de la transmission atmosphérique dans le visible et l'infrarouge a été effectuée au cours de chutes de neige pendant la période mars-avril 1985. Les mesures sont comparées aux transmissions prédites par le module XSALF du "Electro-Optical Systems Atmospheric Effects Library" (EOSAEL). Les prédictions de XSALF correspondent bien aux transmittances mesurées dans le visible mais les prédictions dans l'IR sont considérablement moindres que les valeurs mesurées. Cela suggère que l'algorithme utilisé pour calculer la transmittance dans la neige est plus précis pour les transmissomètres dont le récepteur est beaucoup plus large que le diamètre du faisceau.</p>	<p>CRDV R-4423/87 (SANS CLASSIFICATION)</p> <p>Bureau - Recherche et Développement, MDN, Canada. CRDV, C.P. 8800, Courcellette, Qué. G0A 1R0</p> <p>"Vérification des calculs EOSAEL de transmittance dans la neige" par D. Hutt et R.C. Shirkey</p> <p>La mesure de la transmission atmosphérique dans le visible et l'infrarouge a été effectuée au cours de chutes de neige pendant la période mars-avril 1985. Les mesures sont comparées aux transmissions prédites par le module XSALF du "Electro-Optical Systems Atmospheric Effects Library" (EOSAEL). Les prédictions de XSALF correspondent bien aux transmittances mesurées dans le visible mais les prédictions dans l'IR sont considérablement moindres que les valeurs mesurées. Cela suggère que l'algorithme utilisé pour calculer la transmittance dans la neige est plus précis pour les transmissomètres dont le récepteur est beaucoup plus large que le diamètre du faisceau.</p>

DREV R-4423/87 (UNCLASSIFIED)

Research and Development Branch, DND, Canada.
DREV, P.O. Box 8800, Courcellette, Que. G0A 1R0

"Verification of EOSAEL Snow Transmittance Predictions"
by D. Hutt and R.C. Shirley

Measurements of atmospheric transmission during periods of snowfall were made in the visible and infrared during March and April 1985. The measurements are compared to transmission predicted by the XSCALE module of the Electro-Optical Systems Atmospheric Effects Library (EOSAEL). The XSCALE predictions correspond well with measured transmittances in the visible but predictions in the IR are considerably less than the measured values. This suggests that the snow transmittance algorithm used in XSCALE is more accurate for transmissometers whose receiver diameters are much larger than the beam diameter.

DREV R-4423/87 (UNCLASSIFIED)

Research and Development Branch, DND, Canada.
DREV, P.O. Box 8800, Courcellette, Que. G0A 1R0

"Verification of EOSAEL Snow Transmittance Predictions"
by D. Hutt and R.C. Shirley

Measurements of atmospheric transmission during periods of snowfall were made in the visible and infrared during March and April 1985. The measurements are compared to transmission predicted by the XSCALE module of the Electro-Optical Systems Atmospheric Effects Library (EOSAEL). The XSCALE predictions correspond well with measured transmittances in the visible but predictions in the IR are considerably less than the measured values. This suggests that the snow transmittance algorithm used in XSCALE is more accurate for transmissometers whose receiver diameters are much larger than the beam diameter.

DREV R-4423/87 (UNCLASSIFIED)

Research and Development Branch, DND, Canada.
DREV, P.O. Box 8800, Courcellette, Que. G0A 1R0

"Verification of EOSAEL Snow Transmittance Predictions"
by D. Hutt and R.C. Shirley

Measurements of atmospheric transmission during periods of snowfall were made in the visible and infrared during March and April 1985. The measurements are compared to transmission predicted by the XSCALE module of the Electro-Optical Systems Atmospheric Effects Library (EOSAEL). The XSCALE predictions correspond well with measured transmittances in the visible but predictions in the IR are considerably less than the measured values. This suggests that the snow transmittance algorithm used in XSCALE is more accurate for transmissometers whose receiver diameters are much larger than the beam diameter.

DREV R-4423/87 (UNCLASSIFIED)

Research and Development Branch, DND, Canada.
DREV, P.O. Box 8800, Courcellette, Que. G0A 1R0

"Verification of EOSAEL Snow Transmittance Predictions"
by D. Hutt and R.C. Shirley

Measurements of atmospheric transmission during periods of snowfall were made in the visible and infrared during March and April 1985. The measurements are compared to transmission predicted by the XSCALE module of the Electro-Optical Systems Atmospheric Effects Library (EOSAEL). The XSCALE predictions correspond well with measured transmittances in the visible but predictions in the IR are considerably less than the measured values. This suggests that the snow transmittance algorithm used in XSCALE is more accurate for transmissometers whose receiver diameters are much larger than the beam diameter.

END

6-87

DTIC